Supplement Information for: Consequences of Exchange-Site Heterogeneity and Dynamics on the UV-Visible Spectrum of Cu-Exchanged SSZ-13

Hui Li,[†,‖] Christopher Paolucci,[†,‡,‖] Ishant Khurana,[¶] Laura N. Wilcox,[¶] Florian Göltl,[§] Jonatan D. Albarracin Caballero,[¶] Arthur J. Shih,[¶] Fabio H. Ribeiro,[¶] Rajamani Gounder,[*,¶] and William F. Schneider[*,†]

†*Department of Chemical and Biomolecular Engineering, University of Notre Dame 182 Fitzpatrick Hall, Notre Dame, IN 46556, USA*

‡*Department of Chemical Engineering, University of Virginia, 102 Engineer's Way, Charlottesville, VA 22904, USA*

¶*Charles D. Davidson School of Chemical Engineering, Purdue University, 480 Stadium Mall Drive, West Lafayette, IN 47907, USA*

§*Department of Chemical and Biological Engineering, University of Wisconsin-Madison, 1415 Engineering Drive, Madison, WI 53706, USA*

‖*Contributed equally to this work*

E-mail: rgounder@purdue.edu; wschneider@nd.edu

Contents

S1 Computational Supplementary Information

To generate synthetic spectra, we used AIMD simulations at 300 K to generate a family of structures, TD-DFT calculations to compute excitation spectra at points along those trajectories, and averaging to generate composite spectra. Computational details are given below. For the computations reported here, approximately 20% of the total computational time is used in generating trajectories and 80% in computing the TD-DFT spectra.

	Machine types	
	EMSL (PNNL)	Notre Dame CRC
Processor specs	Intel Xeon processors, 128 GB memory per node, 16 cores per node, connected by FDR Infiniband network (https://www.emsl.pnl.gov/emslweb/instruments/computing-cascade-atipa-1440-intel-xeon-phi-node-fdr-infiniband-linux-cluster)	Intel Haswell processors, 256 GB RAM, 2 × 12 cores per node, connected by non Infiniband connection (https://wiki.crc.nd.edu/w/index.php/CRC_Quick_Start_Guide)
AIMD simulation hours	Each 150 ps AIMD simulation takes about 200 hours using 4 × 16 core machines	Each 150 ps AIMD simulation takes about 275 hours using 1 × 24 core machines
TD-DFT simulation hours	Each 3-step TD-DFT calculation (on one structure) takes about 1-2 hours using 1 × 16 core machines	Each 3-step TD-DFT calculation (on one structure) takes about 2-3 hours using 1 × 24 core machines

S1.1 AIMD computational details

We used the DFT-optimized geometries as initial structures to start the ab initio molecular dynamics (AIMD) simulations. Five independent simulations were performed non-spin-polarized at 300 K for 30 ps at 0.6 fs time step, for a total of 150 ps of AIMD. AIMD simulations for all Cu monomer and Cu dimer site structures are non-spin-polarized. We used the Car-Parrinello molecular dynamics software (CPMD)[1] to perform Born-Oppenheimer dynamics in the canonical (NVT) ensemble. Electron exchange and correlation were described by the generalized gradient approximation (GGA)[2,3] with Perdew-Becke-Erzenhof (PBE)

functional.[4] The ultrasoft Vanderbilt pseudopotential[5–7] was used with a cut off energy of 30 Rydberg (408 eV). The Nose-Hoover thermostat[8,9] was used to reach the target temperature of 300 K. The first Brillouin zone was sampled at the Γ-points only, for the insulator. Electronic energies were converged to 10^{-5} eV for each step of the AIMD. From each of the 5 independent 30 ps AIMD simulations, 12 ps was used for equilibration and 18 ps was used for data extraction.

S1.2 TD-DFT computational details

We used the TD-DFT method with a screened-hybrid exchange functional (HSE06)[10–14] to compute the UV-Vis absorbance spectrum. TD-DFT calculations were performed using the Vienna ab inito simulation package (VASP)[15] version 5.4.1, and the detailed methods are described in the next section. For Cu monomer structures (Z_2Cu para and meta, and ZCuOH) we performed the calculations with doublet spin state (ISPIN=2, NUPDOWN=1). For Cu dimer structures (Figure 4a in main text) we performed either singlet spin state calculations (ISPIN=2, NUPDOWN=0) or triplet spin state calculations (ISPIN=2, NUPDOWN=2), depending on the spin state of the lowest energy optimized geometry.

Using TD-DFT with a GGA functional predicts a close to zero band gap in Cu-SSZ-13 and an LMCT band from 0 to 20000 cm^{-1} (Figure S1). Optics calculation using HSE-generated wavefunctions without TDDFT results in a spectrum with no d-d transitions (Figure S1). A recent study by Ipek et al[16] used a combination of GW0 and BSE equation on HSE-computed wavefunctions, to compute UV-Vis spectrum of Cu(trans-μ-1,2-O_2)Cu and CuOCu dimer in SSZ-13, and obtained absorption peaks at similar energy levels as in Figure 4d. The differences in peak positions and intensities are likely due to the difference in method and the lack of spectrum averaging. This averaging is important because even the least mobile Z_2Cu species exhibit multiple modes of minima.

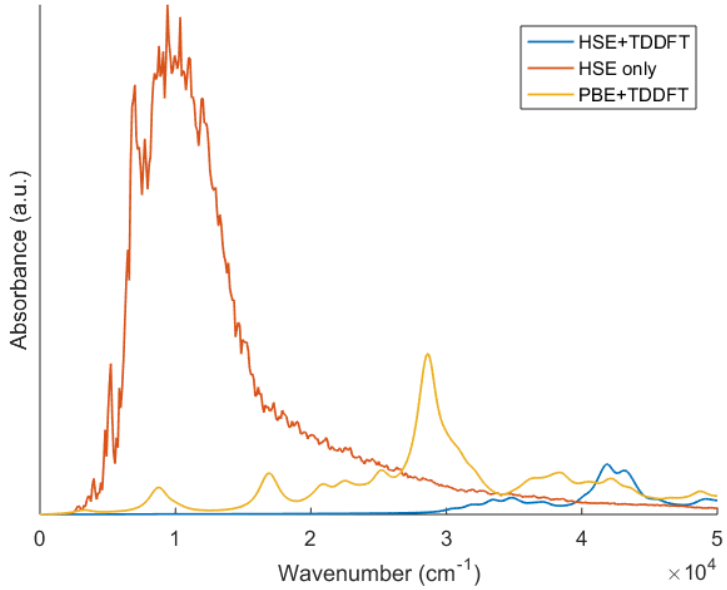

Figure S1: Comparison between UV-Vis spectra calculated at different levels of theory. The blue spectrum corresponds to the black spectrum in Figure 1d in the main text.

S1.2.1 Computational setup for the optical excitation calculations

Optical transitions were calculated using a Time-Dependent HF approach (casually referred to as TD-DFT throughout the manuscript) as implemented in the VASP[15] version 5.4.1. Here the optical response function (i.e. the frequency dependent dielectric function) including excitonic effects is calculated by solving the Casida equation.[17] In the calculations reported here an HSE type hybrid functional[10–14] with an exact exchange contribution of 40% was chosen as wave-function input. This value is close to the expected value for weakly screening materials and close to the value optimized for $CuCl_4$.[18] The calculations are a three step process. In the first step the wave functions for the system are calculated self consistently using the aforementioned functional for a small number of bands. Based on the input wave functions the Hamiltonian is furthermore diagonalized non-selfconsistently for a total of 3072 bands and corresponding wave functions and their derivatives are obtained. Finally optical transitions are calculated for 101 occupied and 200 unoccupied bands. Throughout all calculations energies were converged to differences smaller than 10^{-6} eV, the energy cut-

off was set to 417 eV and the spin states were fixed in the spin ground states of the modeled sites.

In a subsequent step we compared spectra obtained using the TD-DFT method with an HSE functional with 40% exchange to (a) linear response calculations using HSE inputs with 40% exact exchanged and (b) TD-DFT calculations with PBE as an input and (c) GW0 and BSE calculations reported in the literature.[16] Interestingly linear response calculations do not show a significant intensity for the d-d transitions (see Fig. S1). TD-DFT calculations using PBE as a functional significantly red-shift d-d transitions (see Fig. S1), a phenomenon also observed for GW0/BSE calculations in the literature.

S1.2.2 UV-Vis absorption calculation mathematical formula

Using the WAVECAR and WAVEDER files from the previous step, vasp calculates the frequency dependent dielectric matrix ($D(\nu)$) at discrete energy (ν) intervals of 121 cm^{-1} from 0 to 121,000 cm^{-1}. At each energy level (ν) the absorption ($\eta(\nu)$) is then computed to obtain the real (A_{real}) and imaginary (A_{imag}) components of the dielectric matrix ($D(\nu)$). To visualize the UV-Vis absorption, we spline together the $\eta(\nu)$ values at each discrete ν to form a continuous spectrum. η is dimensionless and quatitatively meaningful; it is analogous to units of Kubelka-Munk (K.M.).

$$A_{\text{real}} = \frac{tr\Big(diag\big(real(D)\big)\Big)}{3} \tag{1}$$

$$A_{\text{imag}} = \frac{tr\Big(diag\big(imag(D)\big)\Big)}{3} \tag{2}$$

$$\eta = imag\Big(\sqrt{A_{\text{real}} + iA_{\text{imag}}}\Big) \tag{3}$$

S1.2.3 UV-Vis spectrum calculation and plotting script

This script assumes that there are 400 individual TD-DFT calculations, where 400 real and imaginary dielectric response matrices are extracted from the vasprun.xml files, and placed under folders “real" and “img" respectively.

```
clear all
N=400;
nonzeroentries=N;
aa=[1:1:N];
for ii=1:size(aa,2)
    ranges{ii}=aa(ii);
end
for i=1:N
    dd1=sprintf('img/img%d',ranges{i});
    A1=importdata(dd1);
    dd2=sprintf('real/real%d',ranges{i});
    A2=importdata(dd2);
    if isempty(A1)
        nonzeroentries=nonzeroentries-1;
        continue
    else
        E=A1(:,1);
        Eev=E.*8065.73;
        for j=1:size(A1,1)
            M(1,1)=A1(j,2); M(1,2)=A1(j,5); M(1,3)=A1(j,7);
            M(2,1)=A1(j,5); M(2,2)=A1(j,3); M(2,3)=A1(j,6);
            M(3,1)=A1(j,7); M(3,2)=A1(j,6); M(3,3)=A1(j,4);
            mm(j,1)=sum(diag(M))/3;
        end
        for j=1:size(A1,1)
            R(1,1)=A2(j,2); R(1,2)=A2(j,5); R(1,3)=A2(j,7);
            R(2,1)=A2(j,5); R(2,2)=A2(j,3); R(2,3)=A2(j,6);
            R(3,1)=A2(j,7); R(3,2)=A2(j,6); R(3,3)=A2(j,4);
            rr(j,1)=sum(diag(R))/3;
        end
        tt=imag(sqrt(rr+mm*1i));
        AB(:,i)=tt;
    end
end
Abs=sum(AB,2)./nonzeroentries;
figure;
plot(Eev,Abs);
axis([0 50000 0 -Inf Inf]);
xlabel('Wavenumber (cm^-^1)');
ylabel('Absorbance (a.u.)');
```

S1.3 Calculated Z_2Cu para and meta minima energies

Table S1: Relative energies of the 6 minimum energy structures for Z2Cu.

Al-Al configuration	Minima	Energy (kJ mol^{-1}), relative to lowest energy in all 6 minima	Energy (kJ mol^{-1}), relative to lowest energy in each Al-Al
para	1	5.3	5.3
3NN Al-Al (Fig. 1a)	2	0.0	0.0
	3	0.6	0.6
meta	1	37.3	12.7
2NN Al-Al (Fig. 1f)	2	24.6	0.0
	3	45.1	20.5

S1.4 Cu−O_f distance distributions

Table S2: Cu−O_f distances means and standard deviations (Å) for the histogram analysis in Fig. 2b, Fig. 2f, and Fig 3b.

	first		second	
	Mean (Å)	Standard deviation (Å)	Mean (Å)	Standard deviation (Å)
Z2Cu para (Fig. 2b)	2.08	0.11	3.31	0.15
Z2Cu para (Fig. 2f)	2.09	0.12	3.33	0.16
ZCuOH (Fig. 3b)	1.77	0.04	2.01	0.08

S1.5 Example of intermediate state structure

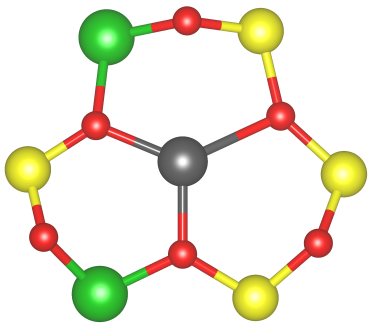

Figure S2: Example of a Z_2Cu meta structure from one of the 400 AIMD snapshots where Cu is only bonded to three first-shell O_f in the 6MR, and does not belong to any of the local minima modes shown in Figure 1e. Structures like this are shown as the white slice in Figure 1f pie chart inset.

S1.6 Boltzmann weighting of spectra

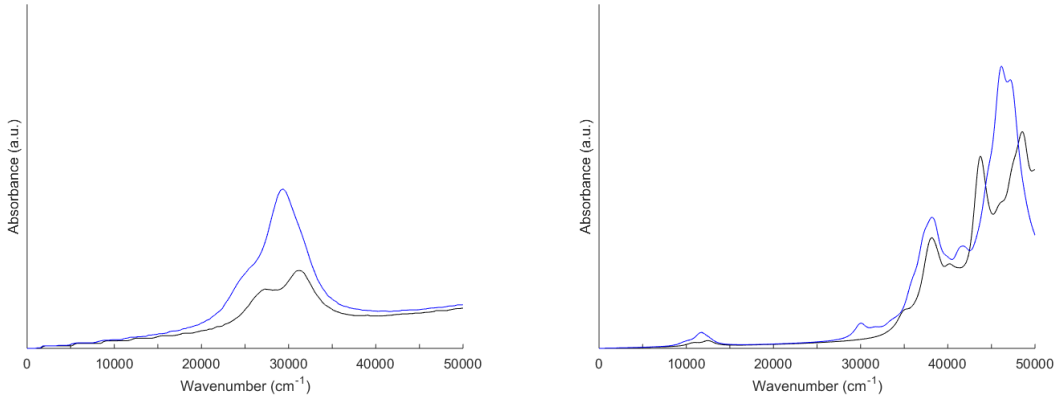

Figure S3: Boltzmann weighted UV-Vis spectra for Z_2Cu para (black) and meta (blue), using the simulated spectra of the 3 minima respectively (Fig. 2c and 2g in the main text). Left panel shows the d-d transition region and the right panel shows the LMCT region.

S1.7 Overlaid 400 UV-Vis spectra

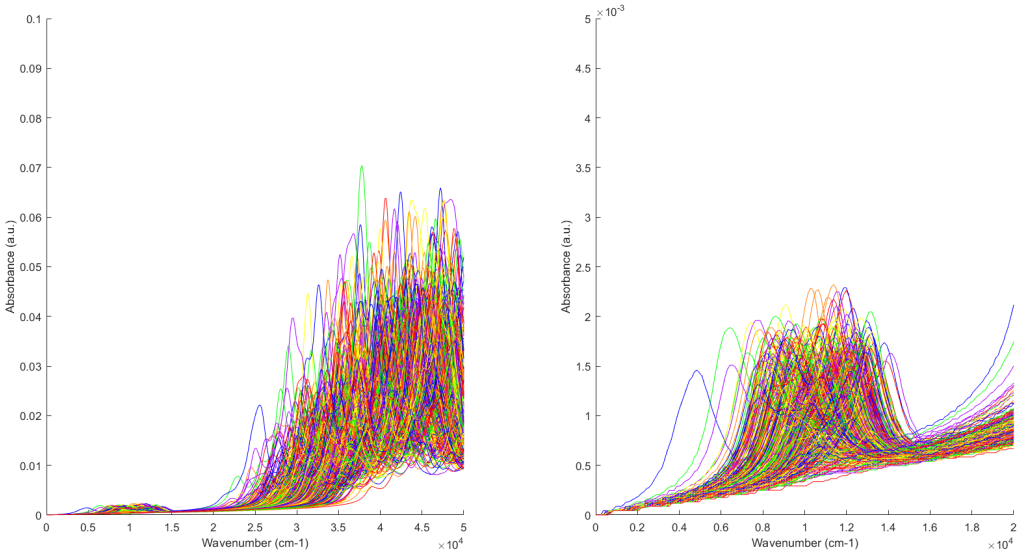

(a) Z_2Cu para

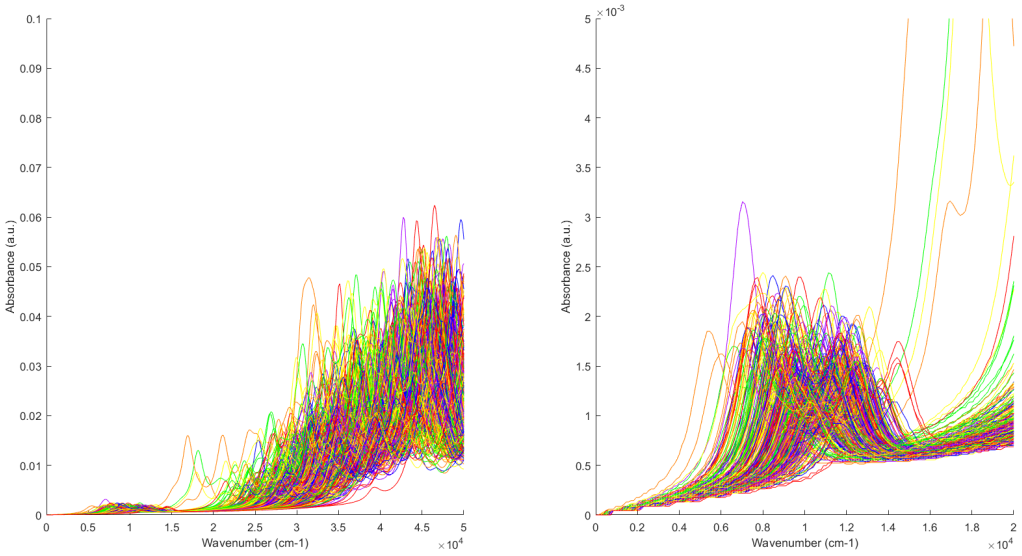

(b) Z_2Cu meta

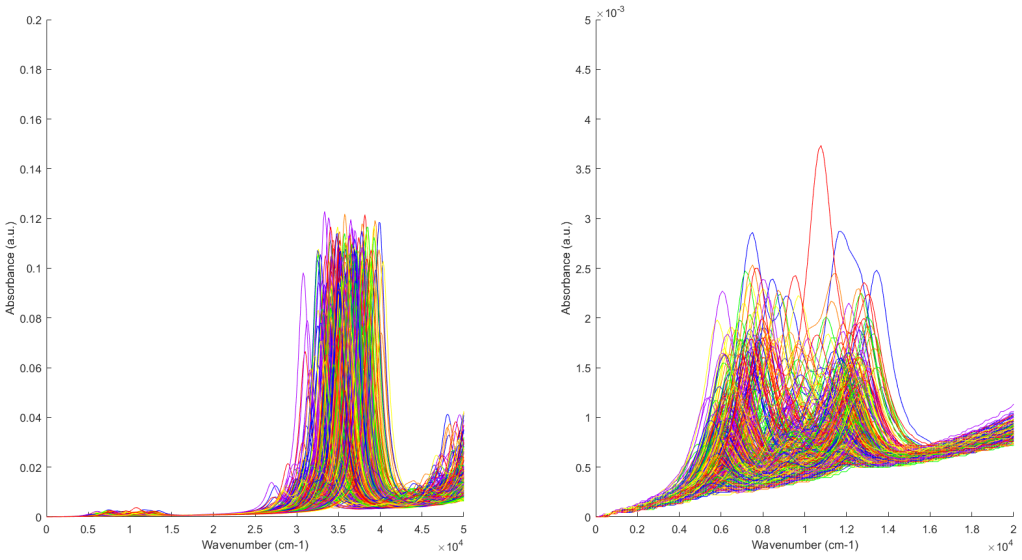

(c) ZCuOH

Figure S4: Overlay of 400 UV-Vis spectra used for averaging, left figures show the 0 to 50,000 cm^{-1} range and the right figures show the 0 to 20,000 cm^{-1} range.

S1.8 d-d transition energy relative to the Cu−O_f distances

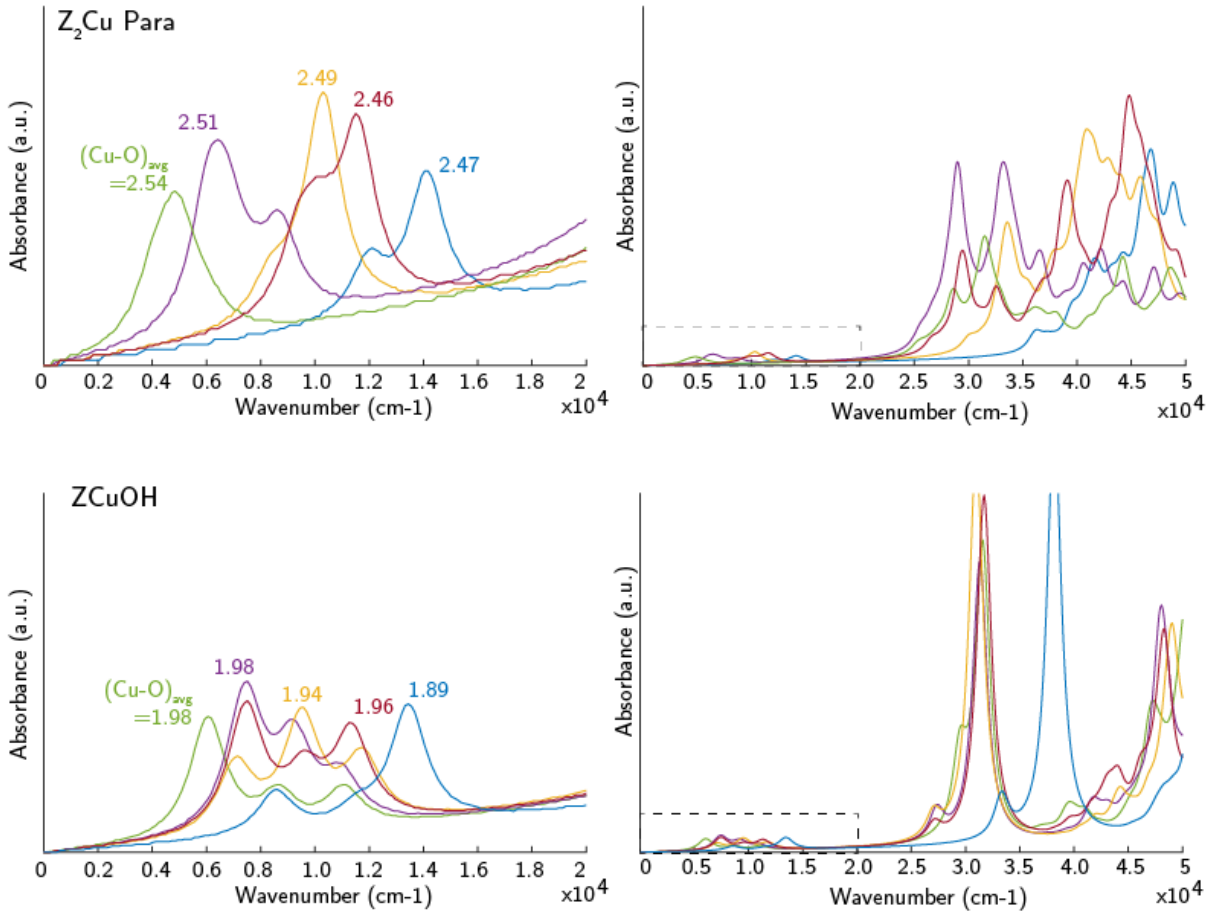

Figure S5: Five representative Z_2Cu para, and ZCuOH UV-Vis spectra from 5 snapshots in the AIMD and the averaged Cu-O distances for each snapshot. Cu-O averages are calculated using the 6 Cu−O_f distances in the Z_2Cu para case, and 2 Cu−O_f plus Cu-O(H) distances in the ZCuOH case. In general the longer the average Cu-O bonds the smaller the d-d transition wavenumber, vice versa.

S1.9 RDF of the 8MR ZCuOH

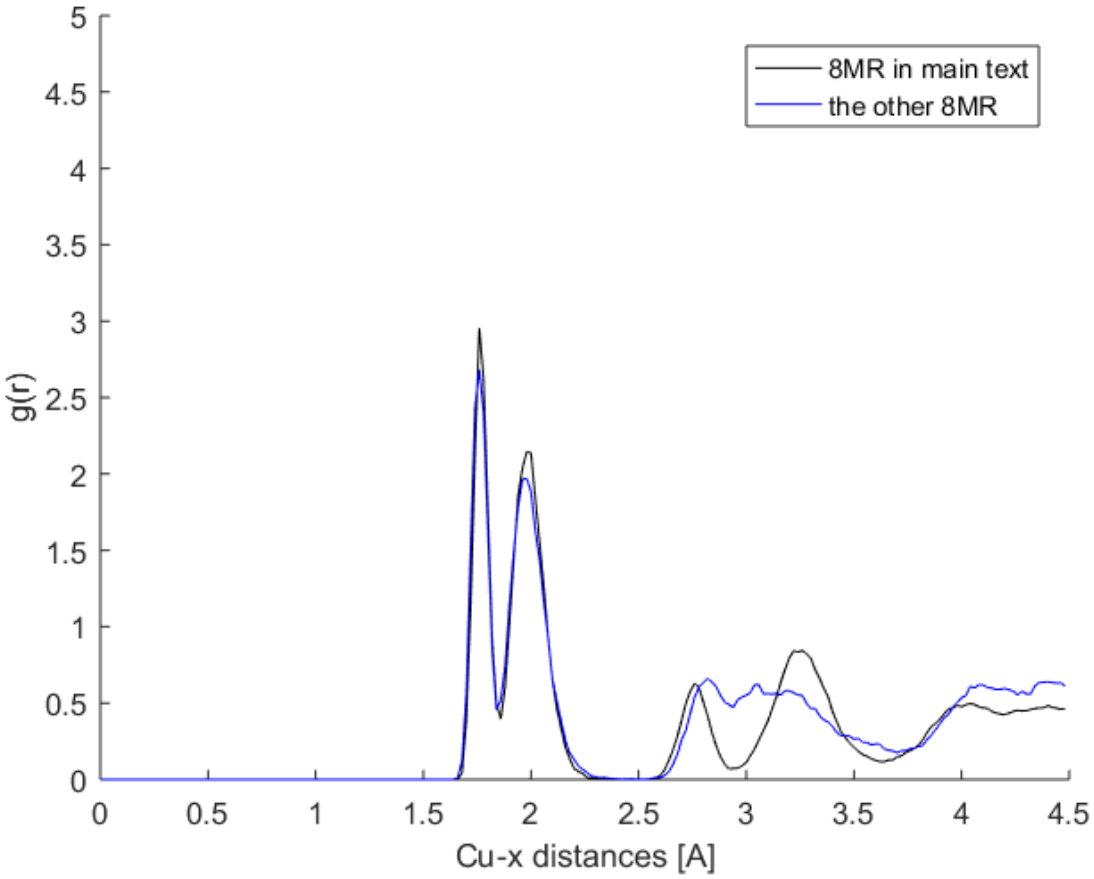

Figure S6: Computed RDF from 150 ps of 300 K AIMDs, for the two different 8MR ZCuOH configurations with the same Al T-site.

S1.10 NEB calculation for $[CuOH]^+$ migration barrier

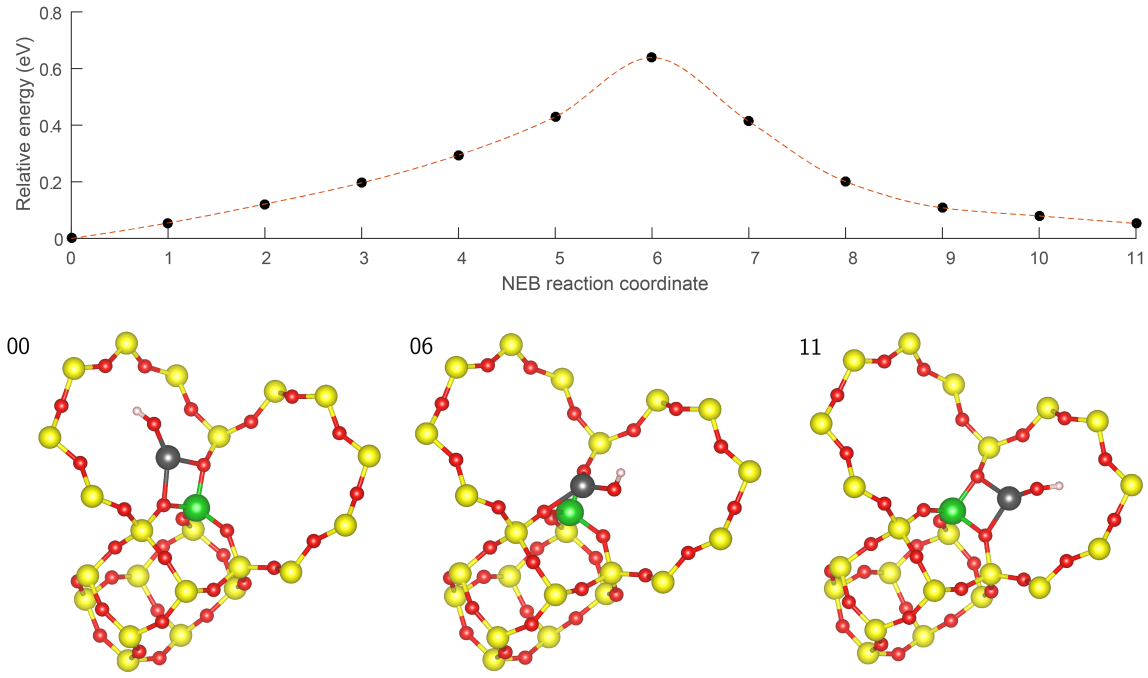

Figure S7: Top: Nudge elastic band (NEB) calculated energy barrier of CuOH switching coordination from one 8MR to an adjacent 8MR. Red dotted curve is the spline interpolation between the relative energy data points and is used only as a guide to eyes. Bottom: Starting (00), transition (06), and ending (11) structures from NEB snapshot images.

S1.11 ZCuO UV-Vis spectrum

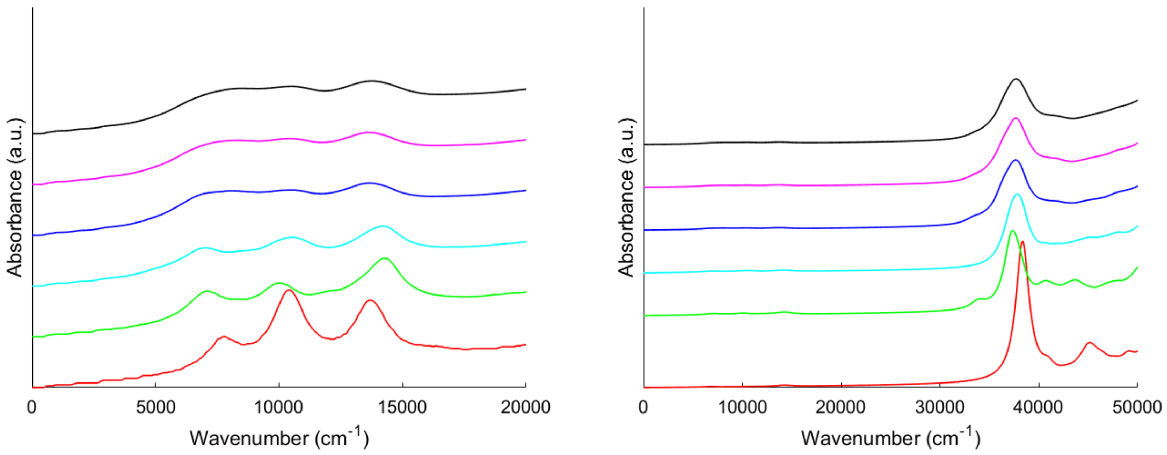

Figure S8: UV-Vis spectrum of ZCuO at 300 K, averaged with 1 (red), 10 (green), 25 (cyan), 100 (blue), 200 (magenta), and 400 (black) structures.

S1.12 Condensation of 2 proximal ZCuOH

To estimate the temperature and water concentration where the two condensation reactions are favorable, we constructed a thermodynamic phase diagram, computed under the same assumptions (Figure S10). Energies were taken from DFT calculated energies in 36-T supercells. The harmonic vibrator approximation was used for formation entropy, and reference chemical potential of H_2O is read from the JANAF table. Condensation to the dihydroxyl dimer $ZCu(OH)_2CuZ$ (Eqn 1) is more favorable at T < 350 K (H_2O =5% -7%), while the CuOCu dimer (Eqn 2) becomes more exergonic above 350 K. Two $[CuOH]^+$ across an 8MR are thus expected to exist as dimers over a wide range of conditions.

$$2\,\mathrm{ZCuOH} \longrightarrow \mathrm{ZCu(OH)_2CuZ} \tag{4}$$

$$2\,\mathrm{ZCuOH} \longrightarrow \mathrm{ZCuOCuZ} + \mathrm{H_2O} \tag{5}$$

Table S3: Computed PBE-D2 energies of the two reactions above.

Reaction	Energy, singlet (kJ mol^{-1})	Energy, triplet (kJ mol^{-1})
(4)	-96.2	-108.7
(5)	46.8	35.3

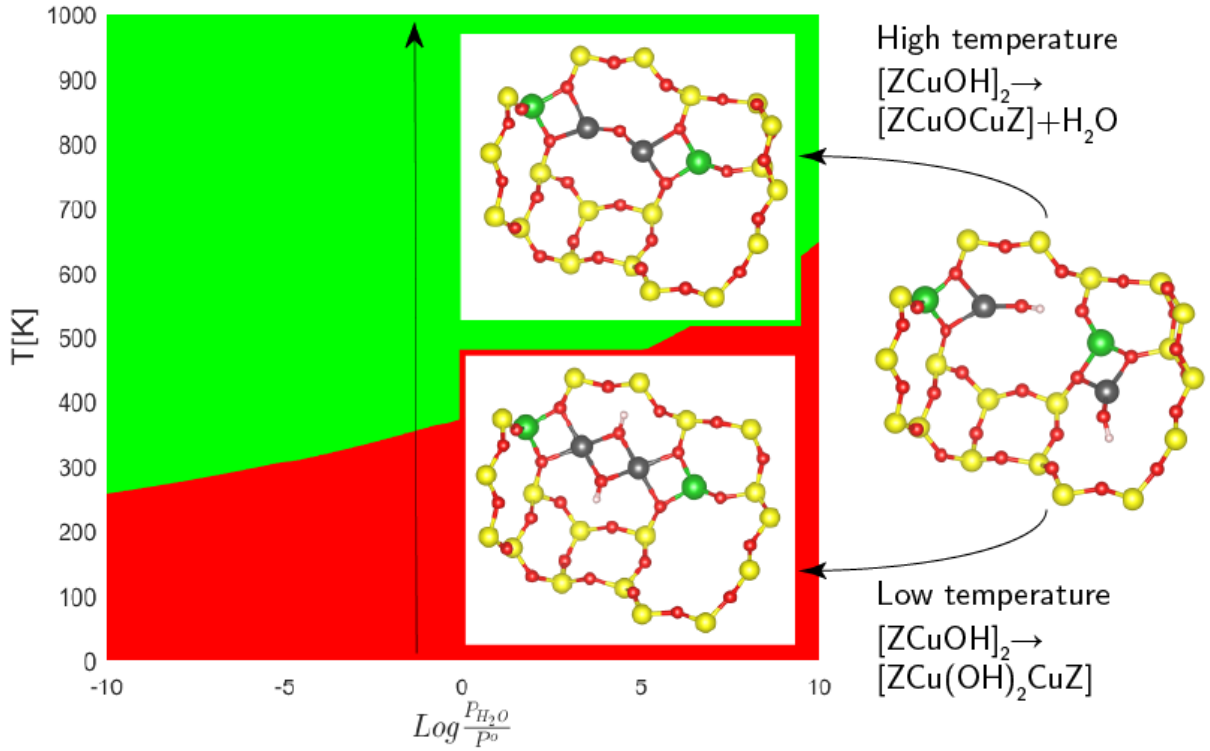

Figure S9: Phase diagram of free energy of formation between ZCuOCuZ ($+H_2O$) and $ZCu(OH)_2CuZ$ dimer species, plotted with respect to temperature and P_{H_2O}.

S1.13 Spectra averaging for dimers A-G

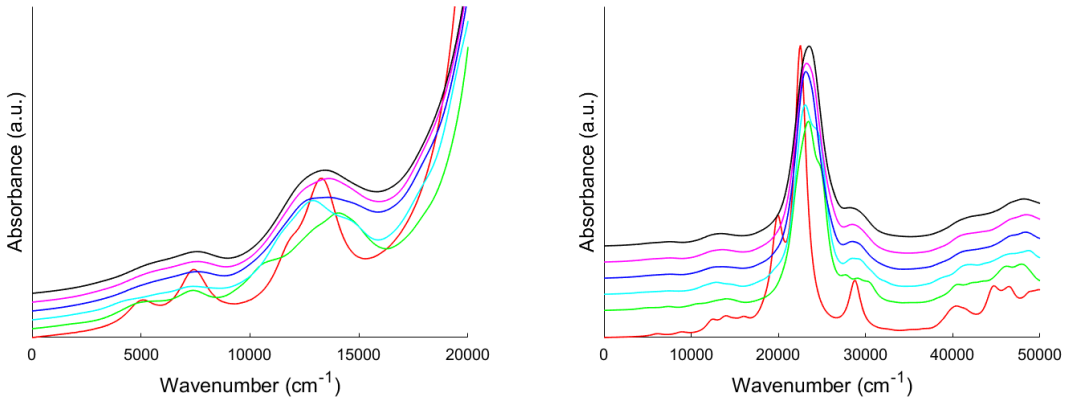

(a) Dimer A

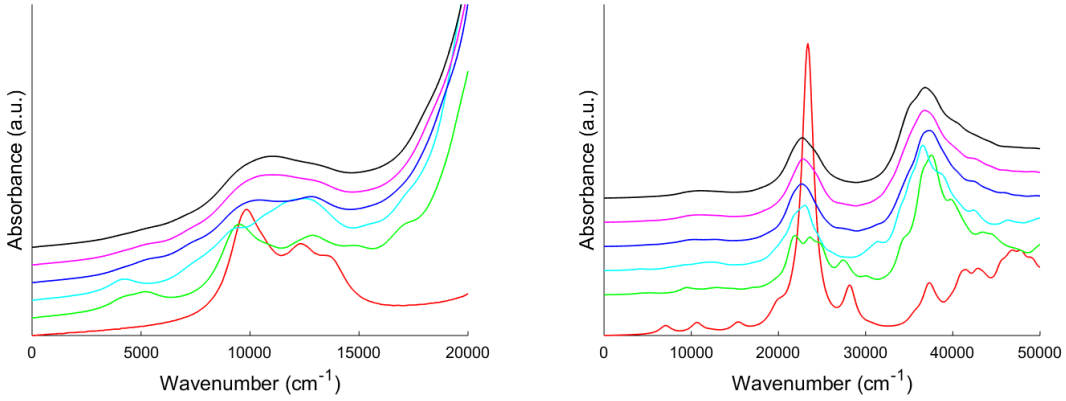

(b) Dimer B

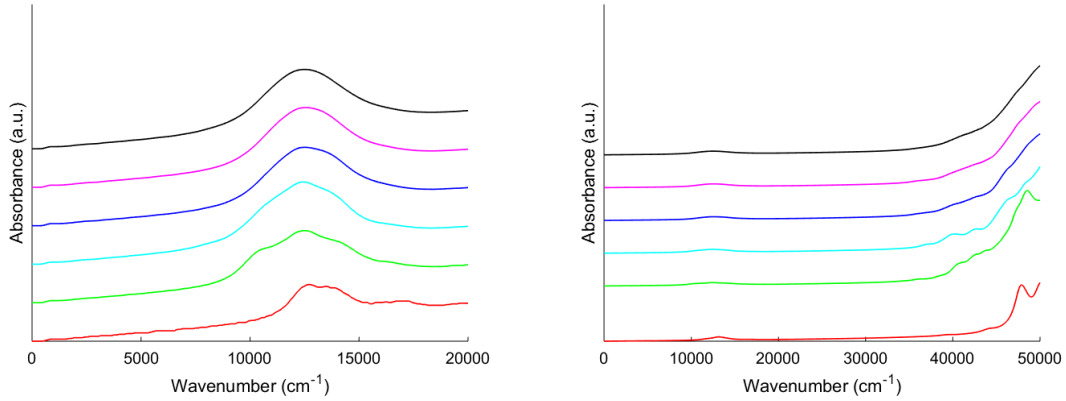

(c) Dimer C

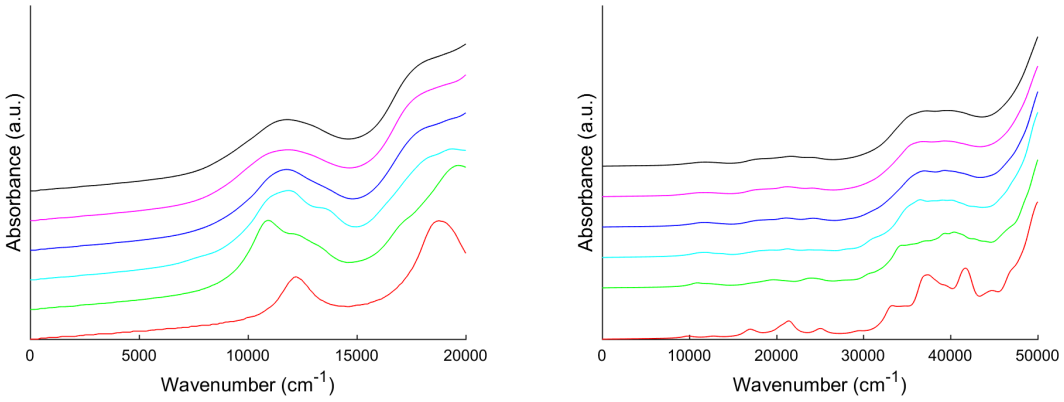

(d) Dimer D

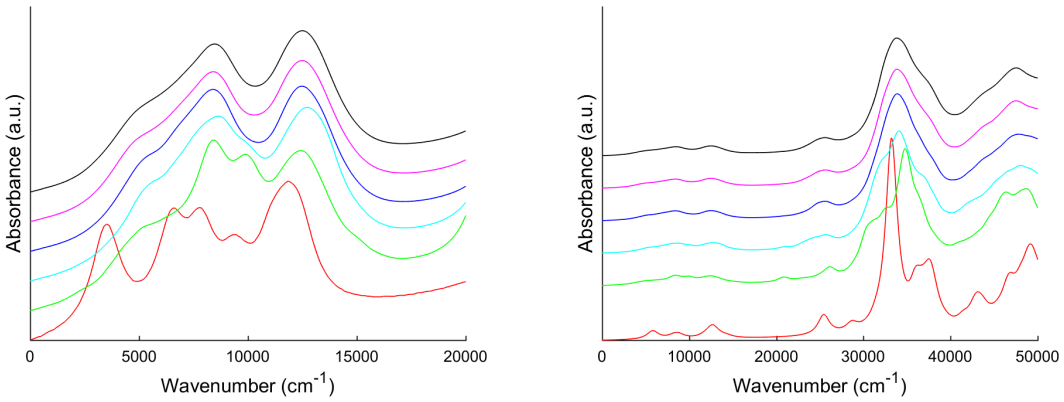

(e) Dimer E

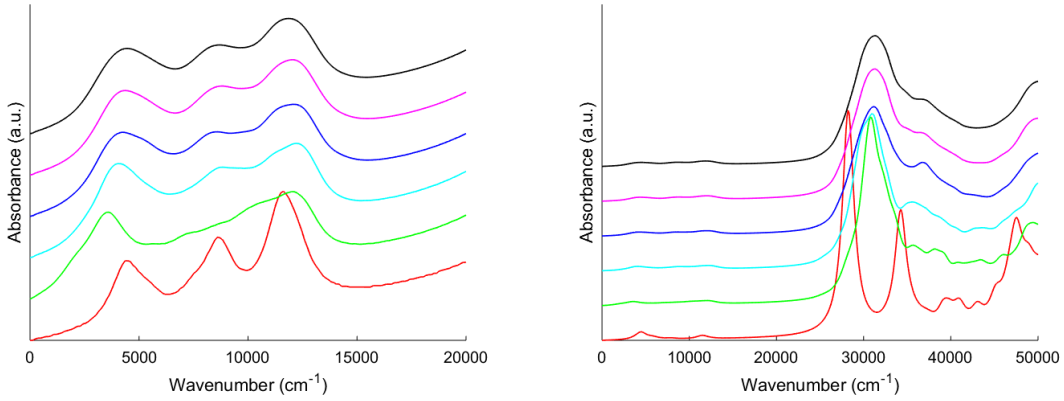

(f) Dimer F

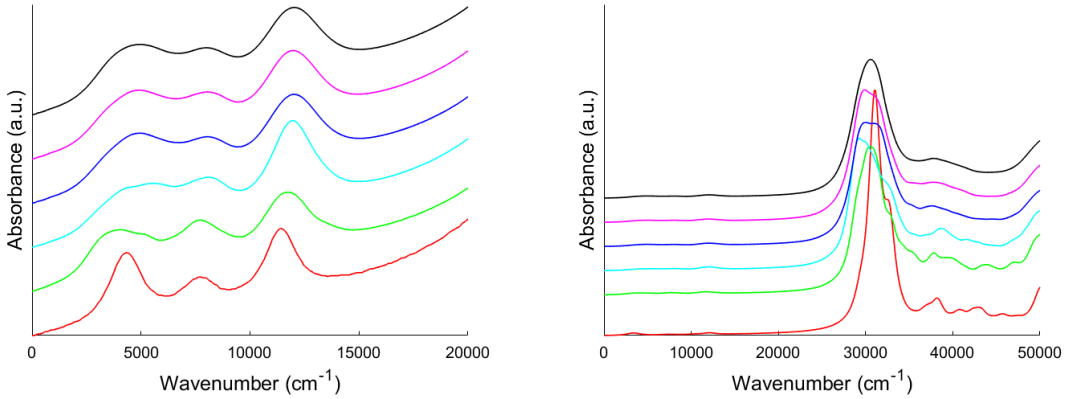

(g) Dimer G

Figure S10: UV-Vis spectrum averaging for dimers in Fig. 4a A-G, with 1 (red), 10 (green), 25 (cyan), 100 (blue), 200 (magenta), and 400 (black) structures, left figures show the 0 to 20,000 cm^{-1} range and the right figures show the 0 to 50,000 cm^{-1} range.

S1.14 Dimer B energy minima

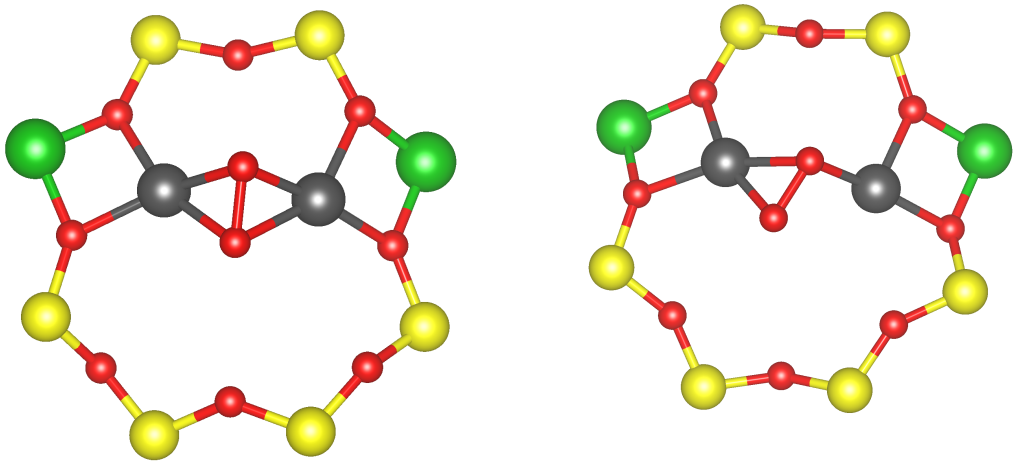

(a) (b)

Figure S11: The two energy local minima structures for dimer B, (a) the lower energy minima, the same as presented in Fig. 4a, (b) the local minima 7 kJ mol higher in energy than (a).

S1.15 Dimer C geometry

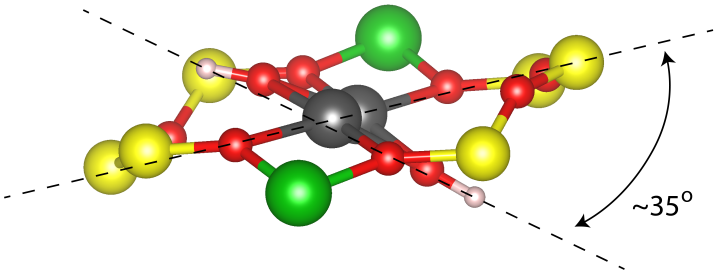

Figure S12: The ≈ 35° angle between the plane of the 8MR and the plane of the $Cu(OH)_2Cu$ core.

S1.16 Dimer A geometry

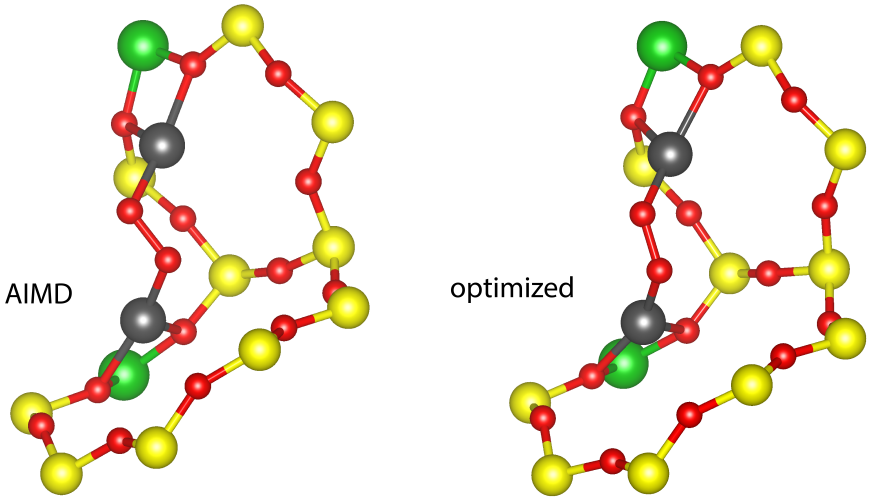

Figure S13: (left) Representative structure of dimer A during AIMD (with smaller Cu-O-O angle). (right) The optimized structure of dimer A.

S2 Experimental Supplementary Information

S2.1 Sample preparation

S2.1.1 Synthesis of SSZ-13 with Si/Al=5

SSZ-13 with Si/Al of 5 was synthesized from a conversion of FAU to CHA with the addition of N,N,N-trimethyl-1-adamantylammonium hydroxide (TMAdaOH) using a method developed by Zones[19] and modified by Fickel.[20] The molar ratios used for the synthesis were 1 SiO_2 / 0.031 Al_2O_3 / 0.77 Na_2O / 0.017 TMAdaOH / 12.1 H_2O. A typical synthesis included the addition of 3.14 g of a 1 M NaOH solution (3.3 wt% NaOH, Alfa Aesar) to 4.82 g of deionized water (18.2 MΩ) and allowed to stir for 0.25 h. Next 24.1 g of sodium silicate (25.6 wt% SiO2, 10.6 wt% Na_2O, Sigma Aldrich) were added to the PFA jar and homogenized for 0.25 h, followed by the addition of 0.37 g of NH4-Y with Si/Al = 2.6 (CBV300, Zeolyst) with additional mixing for 0.5 h. Then 1.58 g of 1 M TMAdaOH (25 wt%, Sachem) were added to the mixture and homogenized for 0.5 h. The solution was stirred under ambient conditions throughout the entire synthesis. The synthesis gel was loaded into 45 ml Teflon liners, encased in stainless steel autoclaves (Parr Instruments), and held at 413 K for 6 days under rotation at 60 RPM in a forced convection oven (Yamato DKN-402C).

S2.1.2 Synthesis of SSZ-13 with Si/Al=15

For the synthesis of SSZ-13 with isolated Al distribution, only $TMAda^+$ was used as a charge balancing cation. To achieve Si/Al of 15, molar ratios of 1 SiO_2 / 0.033 Al_2O_3 / 0.50 TMAdaOH / 44 H_2O were used. In a representative synthesis, 14.07 g of 1 M TMAdaOH solution (25 wt%, Sachem) were added to 12.841 g of deionized water (18.2 MΩ) in a PFA jar and allowed to stir for 0.25 h. Then 0.173 g of $Al(OH)_3$ (98 wt%, SPI Pharma) were added to the PFA jar and homogenized for 0.25 h. Next 5 g of colloidal silica (LudoxHS40, 40 wt%, Sigma Aldrich) were added to the solution and stirred for 2 h. The synthesis solution remained under ambient conditions during the addition and homogenization process. The

synthesis gel was loaded into 45 ml Teflon liners, encased in stainless steel autoclaves (Parr Instruments), and held at 433 K for 6 days under rotation at 40 RPM in a forced convection oven (Yamato DKN-402C).

S2.1.3 Copper Exchange Protocol

The H-form zeolites were copper exchanged using aqueous-phase ion exchange with 0.001 M - 0.1 M $Cu(NO_3)_2$ solution (100 cm^3 g $catalyst^{-1}$; Sigma Aldrich, 99.999 wt%) at ambient conditions for 4 h. The exchange was pH controlled for 4.9 $\pm$ 0.1 with dropwise addition of 1 M NH_4OH (Sigma Aldrich). After exchange, the zeolites were recovered by centrifugation and washed with deionized water six times, dried at 373 K, and then treated in flowing dry air (1.67 cm^3 s^{-1} g $catalyst^{-1}$, 99.999% UHP, Indiana Oxygen) to 773 K (0.0167 K s^{-1}) for 4 h. Elemental analysis was determined using atomic absorption spectroscopy (AAS) with a PerkinElmer AAnalyst 300. Al was measured in a reducing acetylene and nitrous oxide flame at the wavelength 309.3 nm; Cu was measured at the wavelength 324.8 nm in an oxidizing air and acetylene flame. The samples were prepared by dissolving 20 mg of zeolite in 2 g of hydrofluoric acid (48 wt%, Sigma Aldrich), followed by a dilution with 50 g of deionized water.

S2.2 UV-Vis spectroscopy

Diffuse reflectance UV-Visible spectra were recorded under various gas conditions using a Varian UV-VIS-NIR spectrophotometer (Cary 5000) with a diffuse reflectance accessory consisting of two ellipsoidal mirrors (Harrick Scientific Praying Mantis). Barium sulfate (BaSO4, 99.9%, Sigma-Aldrich) was used as the 100% reflectance standard. An in-situ sample holder was loaded with 0.1 g of sample, which was pelleted and sieved to retain particles between 180-250 μm in diameter. Spectra were collected from 7000 to 50000 cm^{-1} with a scan speed of 33.33 cm^{-1} s^{-1}.

S2.3 High temperature O_2 treatment

The sample was dehydrated at 673 K (temperature ramp of 0.5 K s^{-1}) in oxidizing atmosphere of dry air (commercial grade, Indiana Oxygen) with a total flow of 0.833 cm^3 s^{-1} and held at temperature for 2 h. The sample was then cooled to 473 K under the same oxidizing atmosphere, and was further allowed to cool to 300 K. Sample spectra were collected during the cooling steps at 473 K and 300 K.

S2.4 CO reducing treatment

After exposing to high temperature oxidative conditions (673 K in dry air, 2 h), the sample was reduced with 5% CO in balance He (99.999% UHP, Indiana Oxygen) with a total flow of 0.833 cm^3 s^{-1} at 523 K (temperature ramp of 0.5 K s). The sample was exposed to CO until the collected spectra stopped changing, indicating steady state or complete reduction with CO. Then, the sample was flushed with inert He (99.999% UHP, Indiana Oxygen) at 523 K for 0.5 h to remove any physisorbed CO and was further allowed to cool down to 300 K in He flow. The sample spectra were collected during cooling at 473 K and 300 K.

S2.5 Additional table

Table S4: Bulk elemental analysis and fraction of Z_2Cu/ZCuOH sites on the three Cu-SSZ-13 samples.

Type of Cu sites	Si/Al	Cu/Al	Cu wt%	Z2Cu/total Cu	ZCuOH/total Cu
Z2Cu site	5	0.21	3.7	0.21	0.00
ZCuOH site	15	0.24	1.7	0.00	0.24
	15	0.15	1.0	0.00	0.15

References

(1) IBM Corporation, Carr-Parrinello Molecular Dynamics Code, copyright IBM Corp 1990–2016, copyright MPI für Festkörperforschung Stuggart 1997–2001. 2016; `http:`

//www.cpmd.org/.

(2) Perdew, J. P.; Chevary, J. A.; Vosko, S. H.; Jackson, K. A.; Pederson, M. R.; Singh, D. J.; Fiolhais, C. Atoms, molecules, solids, and surfaces: Applications of the generalized gradient approximation for exchange and correlation. *Phys. Rev. B* **1992**, *46*, 6671–6687.

(3) Perdew, J. P.; Burke, K.; Ernzerhof, M. Generalized Gradient Approximation Made Simple. *Phys. Rev. Lett.* **1997**, *78*, 1396.

(4) Perdew, J. P.; Wang, Y. Accurate and Simple Analytic Representation of the Electron-Gas Correlation-Energy. *Phys. Rev. B* **1992**, *45*, 13244–13249.

(5) Vanderbilt, D. Soft self-consistent pseudopotentials in a generalized eigenvalue formalism. *Phys. Rev. B* **1990**, *41*, 7892–7895.

(6) Laasonen, K.; Car, R.; Lee, C.; Vanderbilt, D. Implementation of ultrasoft pseudopotentials in ab initio molecular dynamics. *Phys. Rev. B* **1991**, *43*, 6796–6799.

(7) Laasonen, K.; Pasquarello, A.; Car, R.; Lee, C.; Vanderbilt, D. Car-Parrinello molecular dynamics with Vanderbilt ultrasoft pseudopotentials. *Phys. Rev. B* **1993**, *47*, 10142–10153.

(8) Nosé, S. A unified formulation of the constant temperature molecular dynamics methods. *J. Chem. Phys.* **1984**, *81*, 511–519.

(9) Hoover, W. G. Canonical dynamics: Equilibrium phase-space distributions. *Phys. Rev. A* **1985**, *31*, 1695–1697.

(10) Heyd, J.; Scuseria, G. E.; Ernzerhof, M. Hybrid functionals based on a screened Coulomb potential. *J. Chem. Phys.* **2003**, *118*, 8207–8215.

(11) Heyd, J.; Scuseria, G. E. Efficient hybrid density functional calculations in solids: Assessment of the Heyd-Scuseria-Ernzerhof screened Coulomb hybrid functional. *J. Chem. Phys.* **2004**, *121*, 1187–1192.

(12) Heyd, J.; Peralta, J. E.; Scuseria, G. E.; Martin, R. L. Energy band gaps and lattice parameters evaluated with the Heyd-Scuseria-Ernzerhof screened hybrid functional. *J. Chem. Phys.* **2005**, *123*, 174101.

(13) Heyd, J.; Scuseria, G. E.; Ernzerhof, M. Erratum:âĂIJHybrid functionals based on a screened Coulomb potentialâĂİ[J. Chem. Phys. 118, 8207 (2003)]. *J. Chem. Phys.* **2006**, *124*, 219906.

(14) Krukau, A. V.; Vydrov, O. A.; Izmaylov, A. F.; Scuseria, G. E. Influence of the exchange screening parameter on the performance of screened hybrid functionals. *J. Chem. Phys.* **2006**, *125*, 224106.

(15) Vienna ab-initio Software Package. `www.vasp.at`.

(16) Ipek, B.; Wulfers, M. J.; Kim, H.; Göltl, F.; Hermans, I.; Smith, J. P.; Booksh, K. S.; Brown, C. M.; Lobo, R. F. Formation of [Cu2O2]2+ and [Cu2O]2+ toward C-H Bond Activation in Cu-SSZ-13 and Cu-SSZ-39. *ACS Catal.* **2017**, *7*, 4291–4303.

(17) Casida, M. E. Generalization of the optimized-effective-potential model to include electron correlation: A variational derivation of the Sham-Schlüter equation for the exact exchange-correlation potential. *Phys. Rev. A* **1995**, *51*, 2005–2013.

(18) Szilagyi, R. K.; Metz, M.; Solomon, E. I. Spectroscopic Calibration of Modern Density Functional Methods Using [CuCl4]2-. *The Journal of Physical Chemistry A* **2002**, *106*, 2994–3007.

(19) Zones, S. I. Conversion of faujasites to high-silica chabazite SSZ-13 in the presence of

N{,}N{,}N-trimethyl-1-adamantammonium iodide. *J. Chem. Soc.{,} Faraday Trans.* **1991**, *87*, 3709–3716.

(20) Fickel, D. W.; Lobo, R. F. Copper coordination in Cu-SSZ-13 and Cu-SSZ-16 investigated by variable-temperature XRD. *J. Phys. Chem. C* **2010**, *114*, 1633–1640.